A guide to light-sheet fluorescence microscopy for multiscale imaging

Rory M Power[1–3] & Jan Huisken[1–3]

The impact of light-sheet fluorescence microscopy (LSFM) is visible in fields as diverse as developmental and cell biology, anatomical science, biophysics and neuroscience. Although adoption among biologists has been steady, LSFM has not displaced more traditional imaging methods despite its often-superior performance. One reason for this is that the field has largely conformed to a do-it-yourself ethic, although the challenges of big image data cannot be overstated. With the most powerful implementations of LSFM available to only a few groups worldwide, the scope of this technique is unnecessarily limited. Here we elucidate the key developments and define a simple set of underlying principles governing LSFM. In doing so, we aim to clarify the decisions to be made for those who wish to develop and use bespoke light-sheet systems and to assist in identifying the best approaches to apply this powerful technique to myriad biological questions.

Fluorescence microscopy in concert with genetically encoded reporters is a powerful tool for biological imaging over space and time. Classical approaches have taken us so far and continue to be useful, but the pursuit of new biological insights often requires higher spatiotemporal resolution in ever-larger, intact samples and, crucially, with a gentle touch, such that biological processes continue unhindered. LSFM is making strides in each of these areas and is so named to reflect the mode of illumination; a sheet of light illuminates planes in the sample sequentially to deliver volumetric imaging. LSFM was developed as a response to inadequate four-dimensional (4D; x, y, z and t) microscopic imaging strategies in developmental and cell biology, which overexpose the sample and poorly temporally resolve its processes. It is LSFM's fundamental combination of optical sectioning and parallelization (**Box 1** and **Fig. 1**) that allows long-term biological studies with minimal phototoxicity and rapid acquisition.

The starting point for the design of light-sheet systems should be a specific biological question or application. Indeed, LSFM is particularly suited for construction around the sample, because the decoupled illumination and detection paths of LSFM provide endless scope for customization and because the microscope may be arbitrarily arranged in space. Although commercial systems perform a crucial role in multi-user environments, the most exacting applications require custom solutions (**Supplementary Notes 1** and **2**). The power of the custom approach becomes particularly apparent when the application pushes the limits of the technology, for example for high-speed *in toto* imaging of neural activity[1], cardiac dynamics[2,3], gastrulation in whole embryos[4,5] and physiologically representative subcellular imaging[6]. Likewise, where concessions must be made to sample-mounting protocols to allow normal development of physically sensitive embryos[7–10], the geometric flexibility is crucial (**Supplementary Note 3**), whereas for behavioral studies the ability to spatially[11] or spectrally[12] avoid visually evoked responses may prove invaluable.

Although it is remarkably simple to build a basic light-sheet microscope[13,14], the bewildering array of variants can be intimidating for those looking

[1]Max Planck Institute of Molecular Cell Biology and Genetics, Dresden, Germany. [2]Department of Medical Engineering, Morgridge Institute for Research, Madison, Wisconsin, USA. [3]Department of Biomedical Engineering, University of Wisconsin, Madison, Wisconsin, USA. Correspondence should be addressed to J.H. (jhuisken@morgridge.org).

BOX 1   OPTICAL SECTIONING AND PARALLELIZATION

To understand how LSFM elegantly sidesteps many of the issues that plague conventional microscopies, consider the question: how does microscopy allow us to visualize biological tissues in 4D (x, y, z and t)? A cursory appreciation of optics is sufficient to understand that out-of-focus objects appear blurred. This is why epifluorescence microscopy, which captures volumes as 2D projections, can only achieve high-contrast imaging in thin samples. The acquisition of images without somehow being able to discriminate based on depth reduces biological systems, which are three-dimensional without exception, to a planar representation. Just as tissue can be mechanically sectioned, sectioning can be achieved non-invasively by optical sectioning, which point-scanning confocal and multiphoton microscopies achieve by the removal of out-of-focus signal and by confining excitation to the focal volume, respectively. However, in each case the serial nature of the acquisition process limits the speed with which volumetric data can be collected. Also, crucially, regions that do not direct contribute to the useful signal are exposed repeatedly, which leads to photodamage.

The manner in which LSFM overcomes these limitations is remarkably simple. Taking a wide-field microscope as its basis, the sample is illuminated from the side with a sheet of light, ensuring that signal arises only from in-focus regions (**Fig. 1**), thereby reducing the total exposure. A camera collects the resulting fluorescence signal, sequentially imaging the volume as 2D optical sections, thus parallelizing the imaging process within each plane. As such, the dwell time
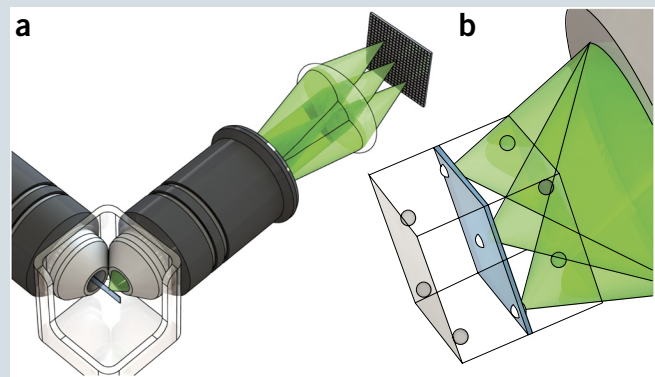

Figure 1 | Light-sheet fluorescence microscopy. (**a**) The archetypal light-sheet microscope: paired, orthogonal optical paths provide plane-wise illumination (blue) and wide-field fluorescence detection (green). (**b**) Optical sectioning by selective illumination of a single plane.

at each point is orders of magnitude higher than that in the point-scanned case, which allows for commensurate reductions in peak light intensity. Because the peak intensity and total power delivered will each have bearing on photodamage rates, the combination of intrinsic sectioning (entire illuminated volume contributes to useable signal) and parallelization (plane-wise acquisition, millisecond exposure times) allow for gentle and rapid imaging. It is this combination of speed, 3D resolving power and low phototoxicity that makes LSFM such an attractive imaging tool to confront a range of biological questions.

to construct and use a bespoke instrument. A range of factors need to be balanced to provide the best possible performance in terms of spatiotemporal resolution, signal-to-noise ratio (SNR) and sample health. Here we give an overview of the state of the LSFM field, providing critical appraisal of the various advances, and note the need for vigilance in ensuring the primacy of the biological system in driving decisions. In doing so the developer is guided through the challenges that are typically encountered in system design, while the user may gain appreciation of the practicalities of LSFM.

A historical perspective is useful in understanding some of the most fundamental choices that need to be made in building or choosing a light-sheet microscope. The first, at least in a form that would be recognizable to a modern user, was developed a little over a decade ago and coined the term selective-plane-illumination microscopy (SPIM). SPIM (**Fig. 2**) illuminates the sample with a static 2D light sheet focused by a cylindrical lens[15], and its use demonstrated for the first time that long-term fluorescence imaging of entire developing embryos could be achieved without unduly impairing their health. As a testament to the strength of SPIM, this fully parallelized scheme (simultaneous whole-plane illumination and detection) has yet to be improved upon for its use in long-term developmental imaging. However, a drawback of illuminating an entire plane at once from the side is the presence of striped artifacts in the resulting data, which arise from refraction, scattering and

absorption of coherent light within tissue. In relatively transparent samples (such as zebrafish embryos), the effects are minimal, but in optically dense samples (such as fruit flies), they may be more severe. A later variant, multidirectional SPIM (mSPIM) (**Fig. 2**), resonantly pivots the light sheet about its focus, illuminating more uniformly and thus reducing the stripe artifacts[16].

Digitally scanned light-sheet microscopy (DSLM) (**Fig. 2**) provides the counter to the full parallelization of SPIM, sweeping out a virtual light sheet by scanning a Gaussian beam through the sample[17]. Because only part of the plane is illuminated at a given time point (i.e., the pixel dwell time decreases), the peak laser power delivered to the sample must increase proportionally to maintain the SNR, thus increasing the chances of fluorophore saturation and rates of photodamage (**Supplementary Note 4**). In optically dense samples, however, DSLM is superior in reducing striping, and the increase in intensity may be manageable even if not desirable (**Fig. 2b**). All light-sheet microscopes are ultimately based on either the SPIM or DSLM architecture, and the choice of whether to scan or not can be crucial in balancing photodamage, imaging speed and quality.

High-resolution imaging

The benefits of LSFM would count for little without being able to compete with, or even outdo, more conventional techniques with regard to spatial resolution (**Box 2**, **Fig. 3** and **Supplementary Note 5**).

a

SPIM/mSPIM

DSLM

☐ Illuminated
▨ Awaiting illumination
■ Inactive

b
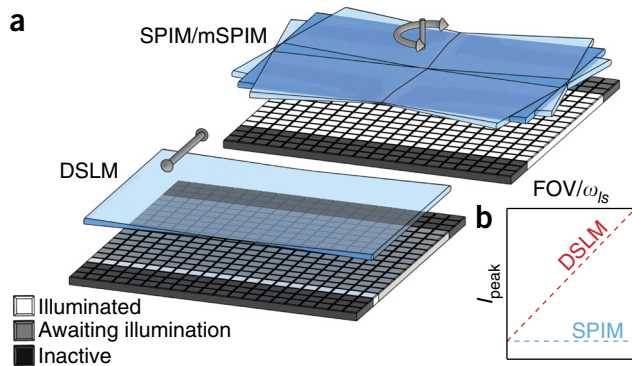
FOV/ω_{ls}

I_{peak}

DSLM

SPIM

Figure 2 | Parallelization of light-sheet generation. (**a**) SPIM illuminates and captures fluorescence from the entire FOV simultaneously, whereas mSPIM reduces striped artifacts by pivoting the light sheet about its center. DSLM produces a virtual light sheet by time-sharing the beam, with fluorescence arising only from the illuminated strip at any given time. (**b**) To maintain identical SNRs, DSLM requires higher peak intensities (I_{peak}) as the FOV size increases (along the scanning axis) relative to the light-sheet thickness, ω_{ls}.

Surmounting the challenges to achieving high-resolution imaging has been the focus of much effort in the light-sheet community, which has spawned a number of approaches. As for all biological imaging, the decision to adopt any one approach should be made with the specific experimental requirements in mind. One should ask how much resolving power is really necessary and should be careful of pursuing extraneous resolution for its own sake. For instance, thinner light sheets (which improve axial resolution) require that a given sample undergo additional exposures to obtain full volumetric coverage.

Microscopy geometry: in pursuit of high resolution. The first challenge for achieving high-resolution imaging in LSFM is largely a geometric issue. High numerical aperture (NA) detection optics are favorable for light-collection efficiency and lateral resolution, whereas high-NA illumination produces thinner light sheets, yielding superior axial resolution and sectioning ability. Unfortunately, concurrent high NA in both pathways is sterically constrained as high-NA lenses are, by necessity, bulky. Although the size of the objective lens, which dictates the achievable NA, requires little consideration in an 'epi' configuration, trying to position high-NA (>0.9) water-immersion lenses such that their orthogonally oriented foci overlap is a fruitless task. Regardless, for many applications, the light-sheet NA (which governs the light-sheet length and thickness) may be much lower, for example, 0.06 > NA > 0.02 is typical to cover a field of view (FOV) of 50–500 µm (λ_{ill} = 488 nm). This permits the use of ultralong-working-distance, low-NA lenses, substantially relaxing the constraints on the choice of objective lens for detection. A summary of objective lenses that are typically used for illumination and detection in LSFM is given (**Supplementary Note 6**) as a guide to what can be orthogonally co-aligned. It is worth noting that some particularly advanced systems have used custom-designed objectives[1,18]; however, the cost and complexity may be prohibitive for the majority of microscopists.

In principle, LSFM provides an ideal platform for far-field super-resolution imaging. In a live-cell context, in particular, the LSFM approach is beneficial relative to near-field techniques

(for example, total internal reflection fluorescence microscopy), which image molecules located within one wavelength of the coverslip. Localization-based techniques exploit the photophysics of molecular probes and allow spatial resolution of tens of nanometers. However, in thick, living samples the indiscriminate nature of the illumination and the numerous exposures required to stochastically construct the image lead to photodamage and out-of-focus signal. By confining the illumination to a thin plane, both can be ameliorated.

In spite of the mutual exclusivity between high detection and illumination NA, a number of localization-based super-resolution light-sheet fluorescence microscopes have been reported. The individual molecule localization selective-plane illumination microscope (IML-SPIM) provides a prime example with a high NA_{det} (1.1) limiting NA_{ill} (0.3)[19]. Although axial localization is achieved through depth-dependent astigmatism[20], the relatively thick light sheet compromises sectioning. Naturally, as one ventures to smaller feature sizes or exceptionally low light levels, the required increase in detection NA eventually becomes a bottleneck, and alternative geometries have to be sought.

To overcome this limitation, Gebhardt *et al.* used a pair of vertically opposed objective lenses with a 45° mirrored cantilever to redirect a thin light sheet (full-width at half maximum (FWHM) thickness of 1 µm) horizontally into the detection plane (**Fig. 4a**), permitting the use of an ultra-high-NA detection objective lens (NA_{det} of 1.4 in oil)[21]. This reflected light-sheet microscopy (RLSM) provides an additional benefit, as the inverted imaging geometry facilitates construction around conventional microscope bodies. Single-objective SPIM (soSPIM) launches the light sheet from the detection objective lens ($NA_{det,max}$ of 1.4 in oil) (**Fig. 4b**). In this case a microcavity mirror coupled to the sample support is used to horizontally reflect the light sheet and deliver similar sectioning to that by RLSM[22]. Because the illumination and detection planes are coupled in soSPIM, the production of volumetric data is more complex and requires a combination of scanning and refocusing. To change the axial position of the light sheet, the beam is swept laterally across the mirror while the detection plane remains co-aligned by translating the objective lens. Naturally, this is accompanied by a shift in the light sheet waist across the FOV. To compensate, an electrically tunable lens repositions the illumination focus. Li *et al.* provided another single-objective variant, termed axial-plane optical microscopy (APOM)[23]. The light sheet is delivered in an epi configuration via an ultra-high-NA (1.4 in oil) objective lens to illuminate a single axial plane. A remotely situated objective and 45°-tilted mirror subsequently serve to rotate and re-image the axial plane onto a camera. Experiments and simulations confirmed that APOM achieved a resolution comparable to that of conventional epi-fluorescence microscopy, although aberrations were incurred toward the periphery of the FOV.

An elegant solution that avoids a reflective element is the so-called π-SPIM, which uses a pair of non-orthogonal objectives (90 < θ < 180) and oblique illumination to relax mechanical constraints somewhat[24], which in essence forms a two-objective variant of a highly inclined and laminated optical sheet (HILO) microscope[25]. Although the obliquity sacrifices some of the illumination objective NA, the geometry allows a combined illumination and detection NA near the theoretical maximum, using only off-the-shelf components (NA_{ill} = 0.71; NA_{det} = 1.1 (water); fill factor = 0.986).

BOX 2   SPATIAL RESOLUTION AND FIELD OF VIEW

The lateral and axial resolution in light-sheet microscopy is determined slightly differently from that of conventional techniques. The product of the illumination and detection PSFs determines the axial resolution. Thinner, high-NA light sheets, therefore, provide superior axial resolution; however, diffraction dictates that a tightly focused (high-NA) Gaussian light sheet diverges rapidly away from the focus (**Fig. 3** and **Supplementary Note 5**). Generally, the region over which the light sheet spreads by no more than $\sqrt{2}$ times the thickness at waist is taken to demarcate the area that is useful for imaging. For a focused Gaussian beam, the resulting light-sheet length, z_{ls}, and thickness, ω_{ls}, are given as:

$$z_{ls} = \frac{2\lambda}{\pi NA^2} \quad (1)$$

$$\omega_{ls} = \frac{2\lambda}{\pi NA} \quad (2)$$

The NA dependence demonstrates that there are diminishing returns on decreasing the light-sheet thickness in terms of the achievable FOV, and so typically some trade-off between usable FOV and axial resolving ability has to be made. Early implementations of LSFM focused on whole-embryo imaging for good reason: isotropic, subcellular resolution requires an ultrathin (high-NA) light sheet, which severely limits FOV.

The theoretically achievable lateral resolution is simply that of a wide-field microscope, governed by the wavelength and NA of the objective lens used for detection. For low magnification-high NA detection lenses, undersampling is frequently employed to sacrifice resolution for FOV. sCMOS (scientific complementary metal-oxide-semiconductor) cameras are generally favored since they deliver ~4–16× larger FOVs (by area) than typical EMCCD

Figure 3 | Spatial resolution in light-sheet fluorescence microscopy. (**a**) Interplay between light-sheet thickness (ω_{ls}) and length (z_{ls}). (**b**) Overlap of illumination (blue) and detection (green) PSFs yields the system PSF. (**c**) Influence of the detection NA on the system PSF, displayed as a summed projection orthogonal to the illumination and detection axes. The color scale defines the normalized intensity of the system PSF.

(electron-multiplying charge couple device) cameras for equivalent spatial sampling. For cases in which FOV is less critical than excellent light sensitivity, EMCCDs may offer a superior solution, notably for super-resolution and multiphoton implementations. Moreover, under light-starved conditions a high-detection NA is favorable, as the collection efficiency scales with NA^2. However, another consequence of high NA is that the DOF of the objective lens will be small, and so only a thin slice of the sample remains in focus. Usually the light sheet has to be thicker to cover the FOV, which compromises the sectioning ability and lowers the contrast.

We note that all of these systems use cylindrical optics to produce the illuminating light sheet, fully parallelizing the acquisition under the inherently low-light conditions. Because low illumination intensities are always desired, one should exercise caution in deviating from this approach.

Light-sheet engineering: in pursuit of high resolution over a large field of view. The second challenge in achieving high-resolution imaging with LSFM is to maintain high axial resolution over a large FOV. Because the overall or system point-spread function (PSF) arises from the overlap of illumination and detection PSFs, isotropic resolution is achievable, in principle, by sufficient axial confinement of the light sheet[26]. Maintaining a thin light sheet across a FOV > 10 μm is problematic, however, as a high-NA Gaussian light sheet spreads rapidly away from the focus. Consequently, the most common light-sheet variants fail to achieve a truly isotropic PSF, and axial resolution is typically no better than ~1 μm (or 2× to 3× worse than lateral resolution) (**Supplementary Note 5**). Although this is perfectly adequate for cellular resolution, it may be limiting for cases in which subcellular resolution is required across a large FOV.
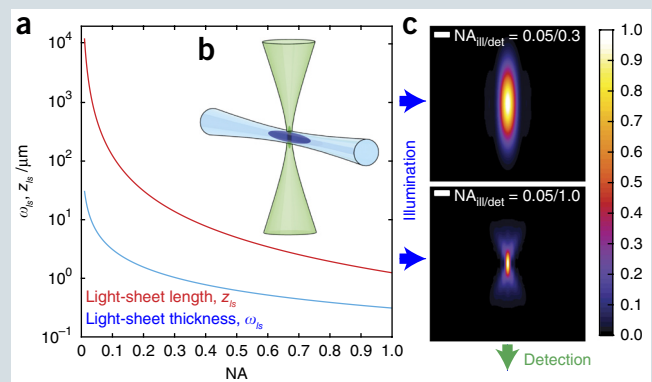
A number of solutions to this problem, using non-diffracting beam modes, have emerged, the most common being the Bessel beam, whose cross-section consists of a narrow central core surrounded by a series of rings of diminishing intensity (**Fig. 5**). These beams are governed by diffraction like any other beam, but they maintain an invariant profile over many times the Rayleigh range of a Gaussian beam of equal NA. Planchon *et al.* used a moderate NA (0.8) in both the illumination and detection pathways to deliver ~300 nm isotropic resolution over a FOV spanning 40 μm along the propagation axis of a scanned Bessel beam[27]. However, the beam side lobes illuminate out-of-focus regions, which compromises sectioning ability, degrades contrast and unnecessarily exposes the sample. By combining with optical-sectioning structured illumination (OS-SIM) or two-photon excitation[6,28], this out-of-focus contribution to the image can be removed or suppressed, respectively, with the caveat that the additional exposures or pulsed illumination increase rates of photobleaching[28]. Additionally, the OS-SIM algorithm produced reconstruction artifacts and discarded a large portion of the useful signal[27]. Gao *et al.* later adapted the technique to utilize super-resolution structured-illumination algorithms (SR-SIM) to provide an improvement in resolution of 1.5-fold to 1.9-fold, an increased
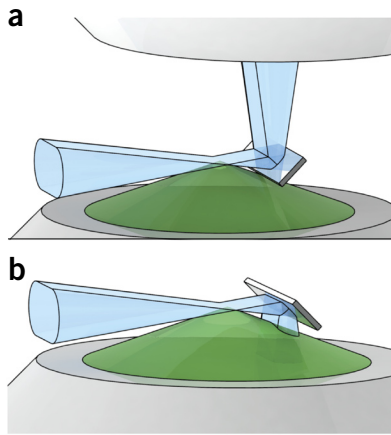
Figure 4 | Reflected light-sheet geometries. (**a**) RLSM—the light sheet is launched from an opposing objective. (**b**) soSPIM—the light sheet is launched from the detection objective.

SNR and a more judicious use of the photon budget[28]. By using multiple Bessel beams in parallel, a commensurate reduction in peak intensity was possible, further reducing photodamage.

Given the correct periodicity, a linear array of Bessel beams may interfere destructively, such that the rings are somewhat suppressed, producing an optical lattice. This realization led to the development of lattice light-sheet microscopy (LLSM), which is capable of delivering ultrathin (FWHM 1 μm) light sheets in a highly parallelized manner[18]. The optical efficiency afforded by this approach coupled with a NA_{det} of 1.1 allowed the electron-multiplying charge couple device (EMCCD) to be replaced with a faster scientific complementary metal-oxide semiconductor (sCMOS) camera. Along with low magnification (25×), the result is a larger FOV than previous Bessel beam implementations[27,28] (~80 × 80 μm) and a plane-wise imaging rate as high as 200 or 1,000 fps (ref. 18) for multi- and single-color imaging, respectively. With the increased detection NA, custom illumination optics were required to maximize the available angular space, delivering a $NA_{ill,max}$ of 0.65.

Two LLSM imaging modes were introduced. In the first case, lattices were designed such that any residual out-of-plane contribution coincides with minima in the detection PSF. The resulting lattices were subsequently dithered to illuminate a single plane. The second, an SR-SIM mode, offered 6.6× faster imaging than the earlier Bessel beam approach[28], with comparable resolution and a ~75% decrease in the total light dose. However, the dithered mode was faster and more compatible with live samples, highlighting the often-damaging effects of pursuing extraneous resolution. The need to project a well-defined pattern into the sample makes LLSM particularly sensitive to degradation of the light sheet, limiting the penetration depth, and thereby FOV, to ~20–100 μm depending on sample opacity. Because resolving the inner workings of single cells can be achieved more simply using other approaches[21,22,24], long-term imaging of small transparent organisms, such as embryonic *Caenorhabditis elegans*, or superficial tissues represents the most promising avenue for LLSM. Nevertheless, it is able to extend localization-based light-sheet imaging to whole organisms, free from the FOV limitations that plague Gaussian-based approaches. A theoretical study

has recently suggested that using three mutually orthogonal objective lenses could further improve the resolution through multiview imaging and interfering lattices[29]. Unfortunately, the optical complexity makes such a scheme difficult to realize. A comparatively simple variant of LLSM has also emerged, which features only physical apertures in place of spatial light modulators (SLMs) to produce a static Bessel light sheet similar in form to the dithered optical lattices[30], although without the side lobe suppression owing to the lattice periodicity[18]. Such a scheme may extend the scope of LLSM by reducing the associated investments in cost and time, although it remains to be seen how the two systems compare.

Other pseudo non-diffracting beams also exist. The Airy mode has been shown to yield thinner light sheets over larger FOVs than Gaussian or Bessel beams of comparable NA[31]. Unfortunately, to allow the beam side lobes to contribute positively to image formation, the data must be deconvolved, requiring that the Airy beam side lobes remain in focus. In turn this has limited the detection NA to 0.4, which is counter to the pursuit of high resolution. For now, the Airy beam remains largely a curiosity, and future studies in a more demanding biological context are welcomed.

Rather than use complicated beam shaping, high axial resolution and large FOVs can be achieved by sweeping a moderate-high NA Gaussian beam through the sample along the propagation axis. Effectively, this approach shares the focus temporally between different focal depths to produce a long and thin light sheet, while sacrificing some (1D) parallelization relative to the analogous SPIM- or DSLM-based approach. Dean and Fiolka, as well as Zong *et al.*, have used ultrasonic lenses to resonantly sweep a focused beam through the sample to achieve sheet thicknesses (FWHM) of 465 nm and 1.5 μm over FOVs of 50 μm and 170 μm, respectively[32,33]. Dean and Fiolka[33] adopted confocal line detection (CLD), which effectively captures the 2D image line-wise to remove out-of-plane contributions from the beam tails (**Fig. 6a**), whereas Zong *et al.*[32] opted for two-photon excitation to suppress out-of-focus contribution owing to the inherent nonlinearity of the process (**Fig. 6b**). Relative to DSLM, the 2D-scan or sweep process and associated decrease in dwell time required higher intensities still, which spurred the development of axially swept light-sheet microscopy (ASLM).
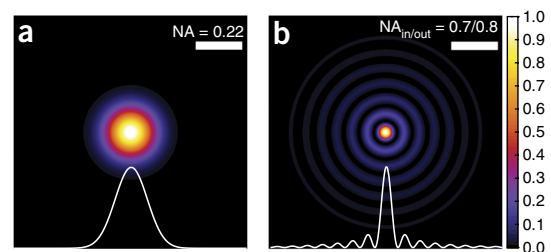

Figure 5 | Gaussian and Bessel beams for light-sheet generation. (**a**,**b**) Gaussian (**a**) and Bessel (**b**) beams produce a light sheet with equivalent length (~6 μm; λ_{ill} = 488 nm; refractive index, n_{imm} = 1.33) despite the disparity in NA. Only a single NA is necessary to define the Gaussian beam, whereas the Bessel beam features two corresponding values that define the inner and outer NA of the annular spectrum of the beam. Although the Bessel beam features a much smaller central beam lobe only, ~11% of the total Bessel beam irradiance is contained therein, and only ~30% is contained within the Gaussian beam waist[105]. The color scale shows the normalized intensity of each of the beams. Scale bars, 1 μm.
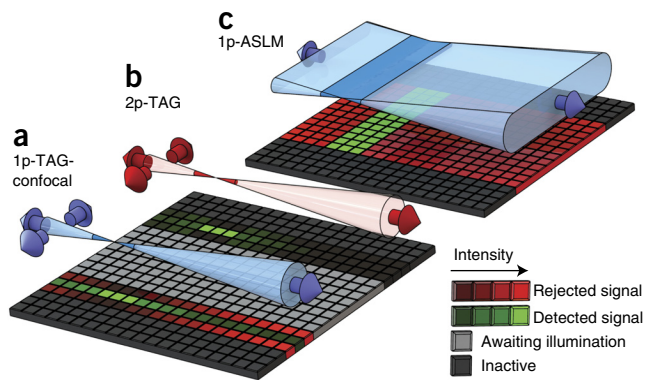
Figure 6 | Axially swept light-sheet geometries. (**a**,**b**) 2D virtual light-sheet production (axially swept or laterally scanned) using ultrasonic (tunable acoustic gradient; TAG) lenses by one-photon excitation with confocal line detection (CLD) to remove undesired signal (**a**) or two-photon excitation to suppress undesired signal (**b**). (**c**) 1D virtual light-sheet production (axially swept) with CLD to remove undesired signal or with sequential acquisition of images at different beam waist positions and subsequent image stitching.

In one sense ASLM is akin to SPIM, producing a short depth-of-field (DOF) light sheet with cylindrical optics (**Fig. 6c**). ASLM sweeps the short light sheet through the sample using a remotely situated objective lens and swept piezo mirror for aberration-free refocusing[34]. Like DSLM, this approach also produces a virtual light sheet in one dimension. ASLM produces ultrathin light sheets over large FOVs by using CLD to remove fluorescence from the beam tails, delivering comparable resolution to LLSM without the need for complicated processing or reconstruction. Illuminating out-of-focus regions is, however, more wasteful with the photon budget.

Tiled acquisition schemes also provide a route to effectively extend the FOV without sacrificing axial resolution, but this has typically involved slow physical translation of optically cleared samples[35], limiting its applicability in a live-imaging context. Gao used an SLM to optically translate a light sheet through the sample in <1 ms, taking images at each position and thus sacrificing speed for spatial resolution[36]. In pursuit of the ideal light sheet, a later incarnation used tiled lattice light sheets, extending the scope of these techniques to larger samples while maintaining subcellular resolution[37]. Perhaps the most intriguing feature, however, is the possibility to tailor the light sheet to the specific needs of the imaging task. For example, taking alternating image stacks with high and low resolution, or adapting the degree of tiling to the sample structure to minimize phototoxicity and provide only the resolution truly required.

Another approach for generating thin and propagation-invariant light sheets is to use molecular dark states. Rather than seeking to overcome diffraction, additional shaped light fields are introduced to inhibit undesired fluorescence emission via a host of molecular processes. Consider the archetypal stimulated emission depletion (STED) microscopy, in which a diffraction-limited focal spot is generated to excite fluorophores while a doughnut-shaped beam depletes the bright state toward the periphery of the excitation focus, permitting lateral super-resolution as the effective focal spot is scanned across a plane. A similar case can be made for light-sheet microscopy with the caveat that the degree of parallelization limits the number of axes that can be super-resolved (one

for static and two for line-scanned). Typically, the high power requirement of STED is at odds with the low-power, gentle acquisition of LSFM[38]. However, a recent study sought to use a reversible saturable or switchable optical (fluorescence) transitions (RESOLFT) strategy, which, while featuring slower molecular transitions that may be limiting in point-scanning microscopies, may be better suited to highly parallelized SPIM-based imaging[39]. The slower switching time allows a commensurate reduction in depletion power, which is more suitable in a live-cell context. In this case, three light sheets were used: the first activated a diffraction limited planar region before a second depleted at the peripheries above and below. The third illuminated the resulting super-resolved photo-activatable region, delivering a 5- to 12-fold improvement in axial resolution.

Large-volume imaging

Since the first development of SPIM, light-sheet methods have shown a tremendous capacity for *in toto* imaging of small embryos and larvae[15]. This is despite the fact that LSFM is unlike conventional techniques, in that degradation of both the illuminating light sheet and fluorescence emission contribute to loss of image contrast. Point-scanning microscopies need only consider the illumination path, as the whole signal is integrated and assigned to a single point. The opposite is true in epi-fluorescence microscopy, which is influenced only by pixel cross-talk in the detection path. LSFM combines the two; the light sheet may broaden with depth in the sample, while cross-talk in the detection path is the inherent trade-off in fully parallelizing the acquisition. Nevertheless, the high SNR and intrinsic optical sectioning of LSFM dominate, yielding high-contrast images. Furthermore, the decoupled illumination and detection paths provide myriad opportunities to further improve imaging at depth, while the efficiency and speed of the imaging process allows a more liberal use of the photon budget in pursuit of improved imaging at depth than could be otherwise tolerated.

Light-sheet engineering: in pursuit of superior penetration. Optical penetration in tissue is primarily governed by scattering and aberrations due to refractive index inhomogeneities, with the mean free path for scattering typically being orders of magnitude shorter than that for absorption. The most common LSFM variants use low-NA light sheets, which show remarkable robustness to aberration, although spreading of the light sheet does contribute to a loss of sectioning and contrast at depth, whereas in-plane scattering contributes to striped artifacts. The desire to limit these effects spawned two-photon (2p) analogs. Because longer wavelengths are more-weakly scattered, the light sheet propagates unperturbed over larger distances, while the nonlinearity of the excitation process improves contrast by limiting the fluorescent contribution from scattered photons. Each scattering event, however, decreases the total fluorescence yield as compared with the linear (single-photon) case, which will continue to evolve signal at depth, although with compromised sectioning (**Fig. 7**).

An early 2p implementation adopted SPIM-type cylindrically focused light sheets[40]; this was not a natural fit because the signal is inversely proportional to the square of the focal volume. Later implementations adopted the DSLM model without exception[12,41–43], providing a convenient compromise between
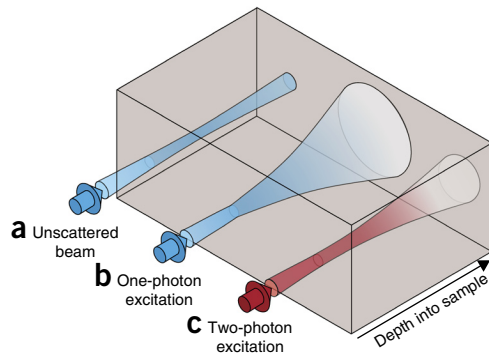
Figure 7 | Light-sheet penetration. Spreading of the beam illustrates the degree of scattering in tissue, and the color opacity illustrates the potential signal evolved. (**a**) The hypothetical unscattered beam is shown for comparison. (**b**) With one-photon excitation, scattering in tissue is severe; however, the signal per unit volume decays linearly as the beam spreads. (**c**) With two-photon excitation, scattering is reduced; however, the signal decays quadratically as the beam spreads.

two-photon laser-scanning microscopy (2p-LSM) and one-photon DSLM (1p-DSLM). Purely on the basis of penetration, 1p-DSLM < 2p-DSLM < 2p-LSM, whereas for the imaging rate, 2p-LSM ≈ 2p-DSLM < 1p-DSLM. The near equivalency between the imaging rates of the 2p systems is perhaps counter-intuitive, but it owes to the scaling of the illuminated volume and signal produced; decreasing the NA_{ill} by a factor of two increases the illuminated volume by 16-fold but equivalently reduces the signal (proportional to NA^{-4} and NA^4, respectively). The caveat is that the weakly focused light sheet has an equivalent reduction in peak intensity and is more robust to aberration. The detrimental effects of intensely pulsed illumination will always be somewhat sample dependent and, although linear photodamage is less problematic when using infrared illumination, nonlinear processes may still contribute to photodamage. For example, structures that absorb light, such as pigmentation, may initiate photodamage, and two-photon imaging of embryos is frequently performed in a pigment-free mutant background[12]. Nevertheless, by spreading the illumination more equitably across time and space, 2p-DSLM reduces nonlinear photodamage relative to that by 2p-LSM, whereas fluorophore saturation, which may ultimately limit imaging speed, is less likely[44].

The comparison of 2p-DSLM with 1p-DSLM is more difficult (**Supplementary Note 4**). Lemon *et al.* provide a comparison for calcium imaging in *Drosophila*, which for one-photon and two-photon excitation led to a ~5% and 20% loss in normalized intensities, respectively, after 5 min of continuous imaging (~20% and 45%, respectively, after 1 h), although 2.5× as many images were recorded in the one-photon case and with 66% higher signal[43]. 2p-LSFM would certainly benefit in the future from strategies that optimize the pulse characteristics in pursuit of reduced photodamage[45]. Multicolor imaging presents an additional challenge for two-photon excitation, requiring multiple expensive pulsed lasers. Mahou *et al.* have demonstrated that a pair of overlapping pulsed lasers is sufficient to excite a third, spectrally intermediate fluorophore[46].

Alternative beam modes may have a part to play in improving the penetration depth in tissue. The delocalization of energy in the outer lobes of the Bessel beam allows self-reconstruction

when scattering objects in the beam path attenuate the central core. Bessel beams have been shown to offer measured improvements in a turbid medium, penetrating 1.55× further into human skin tissue than Gaussian light sheets[47]. Although impressive, the contrast-limiting effect of the concentric side lobes and associated additional photon load discussed earlier are similarly applicable. This may be ameliorated by sectioning the Bessel beam in a manner such that the ring structure is suppressed above and below the imaging plane while maintaining the self-reconstruction ability, although this broadens the resulting light sheet[48]. Similarly, two-photon excitation provides a natural counterpart, further extending the penetration depth and suppressing out-of-focus signal[49]. Two-photon Bessel beams were shown to provide 3.7× superior penetration in multicellular spheroids than the one-photon Gaussian equivalent. However, given that <20% of the total energy may be located in the beam core, the resulting signal may be >18× weaker than the Gaussian case, in which ~85% of the beam energy is contained within the beam waist. Given that two-photon LSFM analogs already operate under extremely low light conditions, little room remains for further losses of efficiency.

In all cases, one must consider the trade-off between enhanced light-sheet penetration and increased photodamage, complexity and expense. In relatively opaque samples such as *Drosophila*, the gains may be significant, whereas they may be outweighed by the costs in optically sensitive or transparent samples, such as *C. elegans* and zebrafish.

Engineering the detection path. Producing high-contrast images at depth requires that the nonballistic (multiply scattered) signal is rejected, either on the basis of response to periodic spatial modulations in the illumination pattern or by spatially filtering the emitted photons. The former is the basis of incoherent structured illumination (SI), in which several images are recorded at different spatial phases of a sinusoidally modulated illumination pattern. The optical properties of the specimen affect the spatial frequency content of the resulting image, and scattered light can be rejected on the basis that it no longer carries the identifying spatial modulation. Keller *et al.* demonstrated that the contrast-restoring ability of DSLM-SI is highly sample dependent, with 82% and 261% improvement relative to that with conventional DSLM in zebrafish and *Drosophila* embryos, respectively, highlighting the difference in optical properties between the two model organisms[50]. Ultimately, the need to project a well-resolved pattern, as well as the sample itself, limit the depth at which SI can be effective. Coupled with the need for additional exposures, the achievable temporal resolution is limited, and the biological function of the sample may be impaired.

Spatial filtering provides an additional mechanism by which non-ballistic signal may be discriminated. In confocal microscopy, the pinhole functions as a 2D spatial filter that effectively removes scattered photons and out-of-focus signal. In contrast, wide-field detection, by its nature, allows no such filtering on the basis of the spatial characteristics of detected light. Construction of the image one line at a time offers a convenient middle ground, and because scanned light-sheet variants already sacrifice some parallelization in favor of the additional flexibility, spatial filtering in 1D along the scan direction (referred to here as confocal line detection (CLD)) is viable. In the simplest case, a single image is recorded for each beam position before stitching them together

to produce a single data set by using a virtual confocal slit[51]; however, recording sequential images is too slow, and physical rejection is preferable. Silvestri *et al.* de-scanned to image the beam position onto a static slit before rescanning onto a CCD camera[52]. A more popular solution is to use the rolling shutter of an sCMOS camera, as first demonstrated by Baumgart and Kubitscheck[53]. In this mode, the beam is scanned across the camera chip, and the exposed pixels move synchronously. Some caveats bear consideration. Changes in refractive index between immersion medium, the sample and its mounting may lead to defocusing or steering of the scanned beam, causing it to deviate from its intended position. Consequently, the slit and beam positions may no longer coincide, resulting in severe loss of signal for deep tissues.

The stability and structure of the Bessel beam makes it an ideal candidate for confocal treatment, as the beam penetrates further into tissue without being unduly perturbed. Fahrbach *et al.* explored the depth-dependent attenuation of signal for Gaussian and Bessel beams, demonstrating that the decay in signal with depth is more severe for the former[51]. It is also worth bearing in mind that the spatial filter is only 1D and so will not remove light that is scattered along the slit axis. Silvestri *et al.* noted that this causes an increase in background signal at depth while the useful signal decreases[52]. In contrast to SI, CLD requires no additional exposures or post-processing steps and has become a widespread and powerful tool for scanned LSFM systems. Recent developments include beam multiplexing to utilize the twinned rolling shutters of the current generation of sCMOS cameras, which delivers higher imaging speed[54], as well as more complex multiview implementations[1,55].

Although SI and CLD are useful for rejecting nonballistic signal, it is worth remembering that extracting useful information from images should always be the goal. Given that the ballistic content of light decays exponentially in turbid medium, the detected signal tends to zero at depths beyond a few mean free paths (the average distance between scattering events), and so scattered signal, which may be of sufficient quality for rudimentary analysis (for example, quantifying expression levels) is lost, making quantitative analysis throughout whole embryos difficult. Far from extending the degree of penetration then, both SI and CLD may actually limit it.

Multiview imaging

Small, optically accessible embryos provide a unique opportunity to study biological development, function or behavior *in toto* with single-cell resolution. Perhaps more than any other area of study, this is where LSFM finds its niche. This success may in part be attributed to multiview imaging. Relative to conventional microscopies, LSFM performs remarkably well at low-to-moderate NA (owing to both general efficiency and axial resolving power derived from overlap of orthogonal illumination and detection PSFs). Correspondingly, samples can be positioned far from mechanically small, long-working-distance objective lenses to allow easy manipulation of, and unparalleled optical access to, the sample. Even so, the speed of LSFM is crucial in allowing multiview imaging; conventional methods are simply too slow to take advantage of the paradigm, even when geometry allows it.

The first aspect of multiview imaging concerns improved axial resolution. Because axial resolution is typically lower than lateral, imaging from two directions (separated by 90°) will produce two data sets, which taken together sample all axes with the best possible resolution. The different viewing angles can subsequently be combined to produce a single data set with improved axial resolution[56]. A number of multiview registration[57] and deconvolution algorithms exist, with the most powerful ones capable of performing real-time processing[58] and requiring fewer views[59]. Two views are insufficient to provide truly isotropic resolution; however, additional views reduce the temporal resolution, unnecessarily expose the sample and encode increasing amounts of redundant information[60].

Large and opaque samples may additionally benefit from the superior sample coverage offered by multiview imaging. Full optical coverage can be achieved, even on distal sides of the embryo, by sequentially recording image stacks from different viewing angles and computationally fusing them to produce a single high-resolution data set[15]. For example, consider an embryo with a degree of rotational symmetry, such as the ellipsoidal *Drosophila* embryo or the spherical zebrafish embryo. As shown in **Figure 8**, the light sheet and imaging optics overlap to provide good optical coverage of a quarter of the embryo; therefore, by taking four views that are spaced by 90° each, the entire sample can be covered. Acquisitions from a few closely spaced angles can also help when the sample exhibits a complex geometry that may be changing during a time-lapse experiment, as these views increase the chance to capture a critical event from the best possible angle.

Because LSFM is so fast and the time between image stacks so plentiful, in the simplest case, multiview imaging can be achieved by rotating the sample between acquisitions. Typically, embryos are mounted vertically in gelated cylinders, which provides physiological conditions for development and allows the sample to be turned without distortion. That being said, rotation of the sample is usually the rate-limiting step and becomes a bottleneck for multicolor, multiview imaging. Even when the sample can be rapidly rotated, it remains to be verified whether the health of the sample is not compromised or the soft embedding required to allow normal development remains structurally sound under the additional strain. A more attractive option is to add additional objective lenses to image the sample.

Multidirectional SPIM (mSPIM) was the first technique to add a second illumination lens, which effectively provides two views of the sample as it is sequentially illuminated from either side[16]. Although synchronous double-sided illumination is possible, this results in a loss of contrast as the light sheet spreads toward the opposing side of the embryo. Because a rudimentary fusion of the two views can be achieved by stitching together the good half of each image, only half of the FOV needs to be covered by each light sheet. As such, each light sheet may be made thinner by a factor of $\sqrt{2}$ without compromising the FOV. Nevertheless, full optical coverage still requires at least one rotation, as half of the embryo remains inaccessible to the single detection path.

Naturally, the addition of a second detection path is the next logical step to further improve optical coverage and eliminate the need for computationally intensive registration of opposing views. This assumes that both cameras see the exact same FOV. Also, as the number of objective lenses increases, the precision required to co-align all of the optical components becomes more exacting. Several solutions to these challenges emerged in quick succession. Krzic *et al.* developed multiview SPIM (MuVi-SPIM),

a scanned light-sheet system capable of providing full 3D coverage of *Drosophila* embryos from four distinct views[61]. Despite the complete optical coverage of the embryo, improvements to axial resolution still required at least a single rotation of 90°, which effectively doubled the imaging time (20 s to 40 s). More recently, Medeiros *et al.* developed a confocal variant, which exploits the attenuation with depth to allow synchronous double-sided illumination[55]; it is notable that the attenuation at the depth associated with two-photon excitation allows the same[41]. Tomer *et al.* reported another scanned implementation, termed simultaneous multiview light-sheet microscopy (SiMView), with both one- and two-photon excitation that is capable of imaging entire *Drosophila* embryos in 30 s (ref. 42) and that uses automated software modules to ensure co-alignment of the light sheet and detection optics.

SPIM-type approaches perhaps lend themselves best of all to long-term imaging of developing embryos. In particular, the zebrafish embryo, which is much larger than the *Drosophila* embryo and whose development proceeds over longer time scales benefits greatly from the decreased photodamage relative to that by scanned approaches. We produced a four-lens SPIM specifically designed to image zebrafish embryos during early development[5]. At this stage, the embryo can be approximated as a layer of cells on the surface of a sphere and the microscope used real-time cartographic projections as a data-compression and visualization tool accordingly. Four views of the embryo were acquired in <10 s, but further increases to image quality were achieved by rotating the sample by 45° to produce eight views.

Space constraints dictate that only a certain number of objective lenses can be co-aligned, as even those with moderate NA typically have an angular extent approaching 90°. In any case, more than four objective lenses make sample mounting and manipulation extremely difficult. Adding further utility requires that the existing lenses be used for both illumination and detection. This permits both aspects of multiview imaging, superior optical coverage and improved axial resolution, to be achieved simultaneously and without the need for sample rotation. Dual-view inverted selective-plane illumination microscopy (diSPIM), which was optimized for the relatively small and transparent *C. elegans* embryo, was the first to do so using just two lenses that sequentially delivered illumination and collected fluorescence to provide isotropic resolution following a deconvolution[9].

The latest iteration of the SiMView architecture, IsoView, allows simultaneous illumination and detection in all four paths, and eliminates cross-talk either spatially, using phase-shifted confocal line detection, or spectrally, by switching between colors in the orthogonal pathways[1]. Both modes require scanning all four objectives to refocus the corresponding detection plane, with the result being that the beam waist of each light sheet is translated an equal distance. Correspondingly, the light sheet is more weakly focused to span the additional distance, compromising sectioning somewhat. Nevertheless, multiview deconvolution produced data sets with a spatial resolution of 2.5 μm or better, even in the center of the *Drosophila* embryo.

Each of the multiview systems discussed may seem conceptually similar, but they differ in their complexity; in each case, the key to success is in the details. In particular, the choice of objective lenses can be crucial in large-volume imaging applications
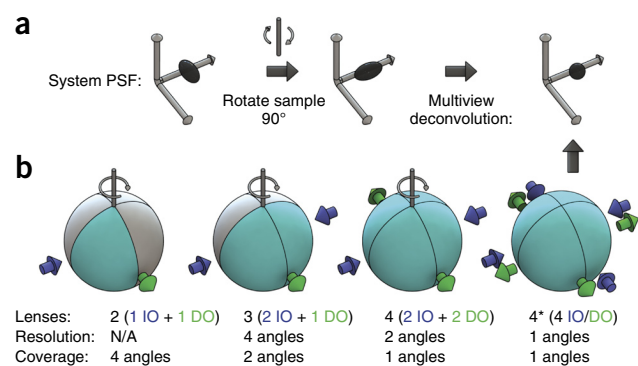
Figure 8 | Multiview imaging. (**a**) Improved axial resolution can be achieved by reconstructing images taken from different angles either achieved by sample rotation (two, three or four lenses) or by using all of the lenses for illumination and detection (4*). (**b**) Optical coverage arises from the overlap of efficiently illuminated and detected quadrants. The (minimum) number of imaging angles to provide full optical coverage and improved axial resolution is given for each case.

(**Supplementary Note 7**). Dealing with the vast amount of data generated by these approaches requires dedicated hardware and software solutions comparable in complexity to the optical engineering itself. Although this aspect lies beyond the scope of this article, it is worth noting that storage, processing, analysis and visualization of tens of terabytes of data is a clear limitation to large-scale uptake of LSFM[5,62].

Optical-clearing optimization of LSFM

Though not specific to LSFM, refractive-index matching by chemical clearing of tissue finds a natural home in this context, which allows for exceptionally large, fixed samples to be imaged with microscopic resolution and in a reasonable period of time. Nevertheless, the transition to larger sample sizes does provide some unique optical challenges, and although clearing makes even deep tissues accessible, without corresponding changes to the optical components they remain tantalizingly out of reach. Dodt *et al.* reported an ultramicroscope that uses low magnification and NA optics to image cleared mouse brains over centimeter-sized FOVs[63] naturally, with some sacrifice to spatial resolution. The generation of thinner, less-divergent light sheets benefits subcellular and macroscopic LSFM imaging alike. Saghafi *et al.* were able to shape the illuminating light sheet using several aspheric and cylindrical lenses in series to produce light sheets with a 4-μm thickness at the beam waist and with little divergence over several millimeters[64]. Others have used binary-pupil phase masks to achieve similar results[65,66]. Tomer *et al.* adopted a different approach to imaging optically cleared tissues in the CLARITY optimized light-sheet microscope (COLM)[67], which tiles the acquisition process to cover large FOVs. The superior collection efficiency afforded by high-NA optics compensates somewhat for the additional exposures by making better use of the available light, whereas the relatively high magnification and NA affords submicron resolution. To compensate for misalignment caused by residual refractive index inhomogeneities deep inside tissue, an autocalibration routine adjusts the light-sheet position such that the two planes maintain co-alignment throughout the volume.

Ultrafast volume imaging

Even in its most basic form, LSFM is fast. With a modern sCMOS camera, this translates to a plane-wise imaging rate of several hundred frames per second. Consequently, volumetric imaging rates in the range of several Hertz are possible in principle, but the motion of the sample through the light sheet becomes mechanically and biologically limiting. This provides the key challenge for ultrafast volume imaging in LSFM. Several contactless solutions have been reported, which allow volumetric imaging without the need for sample movement, and, although differing in approach, all compare favorably to wide-field microscopies using nonselective epi-illumination (**Supplementary Note 8**).

We introduced an electrically tunable lens into the detection path of SPIM (ETL-SPIM)[68] to remotely reposition the detection plane. Synchronous repositioning of the light sheet allows for volumetric imaging free from the translational motion of the sample or objective (**Fig. 9a**). Because SPIM operates far from the photophysical limits of fluorophore saturation, an ultrafast camera was used to image the zebrafish heart beating aperiodically at a volumetric rate of 60 Hz; this is 20× to 30× faster than the beating heart itself and is sufficient to visualize the motion of individual blood cells[3]. After initially being used for developmental imaging, SiMView has since spawned numerous adaptations for the functional imaging of larval *Drosophila* and zebrafish[43,69]. The signals produced by genetically encoded calcium indicators typically decay over time scales of ~1 s, and thus, temporal constraints are sufficiently relaxed for piezo-coupled lenses to provide a practical solution for rapid volumetric imaging. Because inertia becomes a real limitation to mechanically repositioning the objective lens, a custom objective-lens-positioning system based on single-axis piezo stages was developed for a high-speed implementation of SiMView (hs-SiMView)[43]. Using one- and two-photon excitation, volumetric functional imaging of the entire *Drosophila* central nervous system was demonstrated at 2 Hz and 5 Hz, respectively. Imaging of larger specimens, however, is limited by the small travel range of the piezo stages (250 µm) and will probably require alternative strategies.

Fundamentally, the need to reposition the detection focal plane (as in ETL-SPIM or hs-SiMView) is a consequence of the limited depth of field (DOF) of even low-NA objective lenses. Recently, more exotic strategies have emerged for contactless imaging, which aim to extend the DOF of the objective lens; wavefront coding provides such a method to modify the detection PSF. Olarte *et al.* used a deformable mirror to introduce a cubic phase (**Fig. 9b**) in the pupil plane of the detection objective lens to extend the DOF[70]. Consequently, signal from above or below the native detection plane arrived at the camera in focus, although it was shifted and deformed by the modified PSF. To produce meaningful images, the data required deconvolution and transformation. Nevertheless, volumetric imaging up to 10 Hz was demonstrated in live *C. elegans*. A similar scheme was optimized for functional calcium imaging in zebrafish using a static phase mask[71]. Specific neural populations were imaged at 33 Hz by using a random-access scanning routine to acquire images from only a subset of the labeled volume.

In lieu of a phase mask to produce an artificially extended DOF, Tomer *et al.* exploited the spherical aberration introduced by stratified refractive indexes and reported spherical-aberration-assisted (SPED) light-sheet microscopy[72]. Rather than
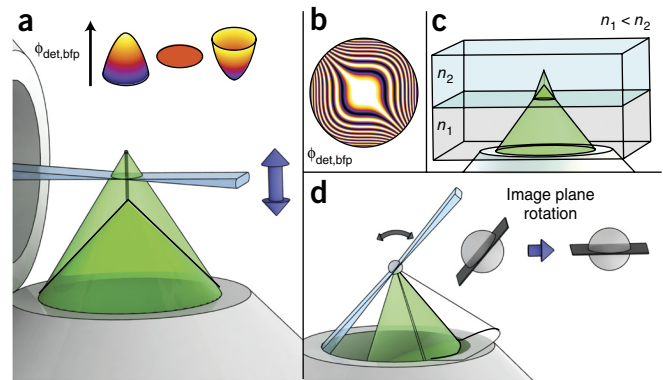

Figure 9 | Ultrafast volumetric imaging. (**a**) Generic scheme for ultrafast light sheet-based volumetric imaging. The light sheet is scanned through an extended DOF. In the case of ETL-SPIM, an extended DOF is produced temporally by a defocusing electrically tunable lens. (**b**) Wavefront coding uses a cubic phase mask to produce a static, artificially extended DOF. (**c**) SPED exploits spherical aberration, which results from focusing through a stratified refractive medium to statically extend the DOF (n_1 and n_2 indicate the refractive index in the first or second immersion medium, respectively). (**d**) OPM–SCAPE uses a tilted illumination and detection scheme alongside image rotation optics for single-objective ultrafast volume imaging.

imaging directly into the sample immersion medium using appropriately corrected objectives, an air-immersion lens was used to provide a variable optical path length through the air or immersion medium to produce a deeper focus for highly inclined rays (refractive indexes: $n_2 > n_1$), effectively extending the DOF (**Fig. 9c**). This effect is largest for high-NA lenses and with a long path through the immersion medium; typically, these two requirements are opposed, requiring some compromise of the NA used. Likewise, a larger refractive index mismatch produces a larger DOF extension; however, this worsens aberrations, as the mismatch between sample and medium increases. Some broadening of the PSF accompanies this treatment, and the data benefit from a subsequent deconvolution. SPED permitted imaging of the entire zebrafish brain or nervous system at 12 Hz and 6 Hz, respectively[72].

The relative merits of the defocus-based (ETL-SPIM, hs-SiMView) or extended DOF (wavefront coding, SPED) approaches can be easily summarized as optical efficiency versus flexibility. The ability to image only selected planes provides a key benefit for DOF-extension methods, which are also less sensitive to illumination-detection misalignments. However, because the detection PSF is delocalized along the detection axis, illumination-detection overlap, and therefore optical efficiency, is drastically reduced relative to the defocus-based methods. Furthermore, for large DOF extensions, high spatial frequency information is lost, limiting resolution[70].

Although the ultrafast schemes discussed so far benefit from maintaining much of the underlying LSFM architecture, others have developed more exotic schemes. The oblique-plane microscope (OPM), developed by Dunsby, uses a single objective lens for illumination and detection[73]. The sample is illuminated obliquely, resulting in a tilted illumination plane. A further pair of objective lenses in the detection path rotates the image plane such that all of the light arrives on the camera in focus (**Fig. 9d**). By scanning one of the remote objective lenses, the illumination and
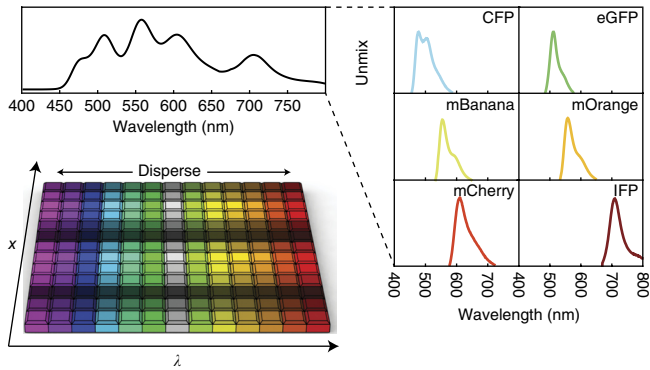
Figure 10 | Hyperspectral light-sheet microscopy. A single line in a multiply labeled sample is illuminated, and the resulting fluorescence is dispersed across the camera chip, encoding spatial (x) and spectral (λ) information. The spectrum at each spatial location (x) is subsequently unmixed to give the contribution from each fluorophore.

detection plane can be shifted synchronously. The impact of OPM, however, has been limited due to the complicated optical configuration and slow objective scanning. Moreover, passing the fluorescence emission via an additional pair of objective lenses wastes signal, and the single-objective scheme, although intriguing, is partially redundant, as the oblique geometry limits the detection NA to 0.7, which is readily attained conventionally. Rather, the power of the approach is to relax steric constraints on sample type and mounting. More recently, the oblique geometry has been revived with the swept confocally aligned planar-excitation microscope (SCAPE)[74], which realizes the full potential of the single-objective approach for imaging large and freely behaving specimens. By eliminating the need to reposition one of the remote objective lenses in favor of a scanning mirror, both the volumetric rate and scan range are improved. Although a theoretical analysis of the imaging performance highlighted a spatially variant, comatic PSF and NA limitations (aspects shared with OPM[74]), the single-objective geometry allowed 3D imaging of the brains of head-fixed behaving mice at volumetric imaging speeds as high as 10 Hz or of freely moving *Drosophila* larvae at 20 Hz[74].

Many biological processes involve a large number of components, and understanding their interplay is crucial. An often-neglected aspect of ultrafast imaging is multicolor acquisition. Typically, multicolor imaging involves sequential acquisition with filters, multiple cameras or image splitters to image two to three spectral bands side by side on a single camera chip. However, for large numbers of closely spaced bands, this is both time-consuming and wasteful, as the overlapping spectral bands cannot be effectively discriminated. Hyperspectral approaches offer an alternative by which the entire spectrum can be captured simultaneously. Because scanned light-sheet variants use only a single strip of the camera chip at a time, the remaining lines may be used to encode spectral data. We have demonstrated this concept, using descanned detection via a confocal slit and diffraction grating onto the camera chip[75]. The resulting 4D image stack (x, y, z and λ) (**Fig. 10**) was linearly unmixed to retrieve the contribution from up to five fluorophores, plus autofluorescence, in zebrafish and *Drosophila* embryos. More recently, seven fluorophores have been separated in zebrafish using hyperspectral confocal microscopy and a spectral-phasor-based approach. Unmixing

in Fourier space was shown to be superior under the inherently noise-limited conditions and should prove powerful in a biologically gentle LSFM context[76]. In principle, many more fluorophores could be imaged simultaneously to deliver a multitude of information from a single sample. One expects that as genetic-editing tools progress, the utility of these approaches will increase.

Toward the future of LSFM
Optically, at least, LSFM is fairly well optimized, comprising a broad toolbox of innovations. However, adaptive optics (AO), which is transforming more conventional fluorescence microscopies[77], presents a large gap in the repertoire despite some limited attempts[78,79]. AO refers to various methods for wavefront control by which optical aberrations and scattering may be pre-compensated. The underlying explanation for the absence is that the union of classical AO and LSFM is not a natural one. Aside from the decoupled illumination and detection pathways, both of which contribute to image formation and need to be considered in principle, the highly parallelized nature of LSFM and the FOV limitations of most AO schemes are diametrically opposed. As such, a fully adaptive light-sheet microscope will most likely require multi-conjugate AO using a large number of wavefront-correcting devices (each conjugate with a different layer of the specimen) to effectively produce an inverse refractive map of the sample and yield a large volume correction[80].

Until such multi-conjugate approaches become technically feasible, a more pragmatic option is to provide a partial correction to simply ensure that the light sheet and detection plane remain co-aligned throughout the FOV. The AutoPilot framework paired a real-time optimization algorithm to a SiMView microscope that featured individually addressable control of the illumination and detection focal position (adapting to defocus) and light-sheet directional properties (adapting to steering or refraction of the light sheet)[81]. Although requiring additional exposures to perform the optimization, <5% of the total experimental time was required to improve the resolution and signal strength in *Drosophila* and zebrafish by twofold to fivefold. This is particularly beneficial for developmental imaging due to the spatiotemporally varying refractive index profile of the sample. Nevertheless, with sparse temporal sampling, the additional exposures may account for a significant portion of the total photon budget. Also, without higher-order wavefront control, the AutoPilot framework simply cannot account for scattering deep within tissue. Because little additional hardware is required, the strength of AutoPilot lies in its applicability to a range of light-sheet systems.

A recent perspective discussed our vision for a future of smart microscopy[82]. Some inroads have already been made in the directions we envisaged, beyond the immediate sphere of LSFM. For example, the concept of controlled light exposure that was developed for confocal microscopy could be useful in LSFM[83]. This could enable automated metering of the light dose in dynamic, developing organisms, thus adapting the image acquisition to the spatiotemporal fluorophore distribution to deliver illumination when and where most appropriate. Conrad *et al.* reported multiresolution sampling using the computational platform MicroPilot to detect biological features of interest and to image accordingly[84]. Limited comparable progress has been made in LSFM, although Chmielewski *et al.* reported a scheme to rapidly

position a light sheet with tunable length and thickness anywhere within the sample, which, appropriately automated, could afford a smart, sample-adaptive illumination scheme[85].

The maintenance of physiologically relevant conditions has long been a hallmark of LSFM and should continue to influence microscope design in the future. Nevertheless, one may question the biological relevance of studying chemically or physically immobilized living systems. Indeed, far from the thin and fixed sample, 3D imaging of freely moving specimens is increasingly a reality, with 3D imaging of freely moving *C. elegans*[86] or *Drosophila*[74,87] embryos having been reported. The challenge for the future is to allow the sample to explore its environment and image its interactions sufficiently quickly to provide a volumetric snapshot, free from motion artifacts.

Truly systematic studies of sample-to-sample variability will require the development of new hyper-dimensional, high-throughput approaches. LSFM lends itself particularly well to flow-through imaging. Indeed, large-scale phenotyping or drug screening in living embryos could be made possible by combining flow-based technologies with LSFM, providing additional power over previous implementations using conventional techniques[88–90]. Gualda *et al.* have taken a step in this direction, with SPIM-fluid capable of 3D high-throughput flow-based imaging of zebrafish embryos[91]. Others have imaged *Drosophila* and zebrafish embryos in microfluidic channels and multiwell plates, respectively, using fluidic optics in the detection path to correct for aberrations resulting from the imaging geometry[87]. Combined with omnidirectional imaging approaches, the potential of such technologies cannot be overstated. However, given that LSFM already pushes the storage capacity of even well-equipped facilities, this will require a rethink as to how data is managed. Dimensional reduction based on cartographic projections provides one such solution in cases for which the tissue structure can be well defined[5,92].

With the advent of 3D micromachining and printing, a growing democratization of light-sheet imaging is under way. Guan *et al.* produced a plane-illumination plugin for conventional wide-field microscopes with an option for dual-sided illumination[93]. Given the number of epifluorescence microscopes in service, such a device illustrates that the absence of commercial light-sheet systems in smaller and less well-funded departments need not limit the access of the greater biological community to what can be a highly cost-effective imaging technology. Paiè *et al.* went one step further and incorporated the light-sheet launcher, which was based on an optofluidic cylindrical lens, into a microfluidic chip[94]. Engelbrecht *et al.* used a microprism-based reflective scheme and gradient index lenses[95], whereas Plöschner *et al.* used a multimode fiber to deliver holographically shaped Bessel beam light sheets[96]. Because the footprint of these devices is small, light-sheet-based endoscopy may become viable.

Fluorescence provides the dominant contrast in light-sheet microscopy, and although Raman and elastic scattering analogs exist[97–99], other modalities may provide information that is otherwise 'left on the table'. In developmental biology, in particular, fluorescence imaging may take up a very small portion of the total time series. In such a case, optical projection tomography (OPT) can provide a transmission contrast to yield a 3D physiological context. Mayer *et al.* reported OPTiSPIM, a low-NA,

hybrid instrument optimized for cleared macroscopic samples[100]. Unfortunately, the requirements of high-resolution LSFM and OPT are not necessarily so well aligned. Typically, one desires the mutually exclusive combination of high NA for efficient fluorescence collection and low NA for a large depth of field in transmission. As a solution, Bassi *et al.* moved the sample through the focal plane to follow a spiral trajectory, allowing NA as high as 0.3 as an efficient compromise[101]. The power of this approach was exploited in developing zebrafish embryos, which provided a structural context to the fluorescence signal. Similarly, magnetic resonance imaging (MRI) has been used to visualize the anatomy of whole mouse brains that are inaccessible to optical imaging following tissue clearing and that is subsequently co-registered with LSFM data to image neural stem cell innervation[102]. A number of optical manipulations are compatible with LSFM, including optogenetics[2,3], laser ablation[103] and even trapping of small microorganisms up to 100 µm in size[104], which should provide additional capabilities in the future.

Future innovation aside, LSFM is now an important optical imaging technique and a mature technology in its own right. It is reasonable to expect that as time goes on, LSFM will continue to replace more established technologies in line with the growing need for fast and gentle imaging of whole organisms, tissues and cells alike.

Note: Any Supplementary Information and Source Data files are available in the online version of the paper.

COMPETING FINANCIAL INTERESTS
The authors declare competing financial interests: details are available in the online version of the paper.

Reprints and permissions information is available online at http://www.nature.com/reprints/index.html.

1. Chhetri, R.K. *et al.* Whole-animal functional and developmental imaging with isotropic spatial resolution. *Nat. Methods* **12**, 1171–1178 (2015).
2. Arrenberg, A.B., Stainier, D.Y.R., Baier, H. & Huisken, J. Optogenetic control of cardiac function. *Science* **330**, 971–974 (2010).
3. Mickoleit, M. *et al.* High-resolution reconstruction of the beating zebrafish heart. *Nat. Methods* **11**, 919–922 (2014).
4. Rauzi, M. *et al.* Embryo-scale tissue mechanics during *Drosophila* gastrulation movements. *Nat. Commun.* **6**, 8677 (2015).
5. Schmid, B. *et al.* High-speed panoramic light-sheet microscopy reveals global endodermal cell dynamics. *Nat. Commun.* **4**, 2207 (2013).
6. Welf, E.S. *et al.* Quantitative multiscale cell imaging in controlled 3D microenvironments. *Dev. Cell* **36**, 462–475 (2016).
7. Strnad, P. *et al.* Inverted light-sheet microscope for imaging mouse pre-implantation development. *Nat. Methods* **13**, 139–142 (2016).
8. Wu, Y. *et al.* Inverted selective-plane illumination microscopy (iSPIM) enables coupled cell identity lineaging and neurodevelopmental imaging in *Caenorhabditis elegans*. *Proc. Natl. Acad. Sci. USA* **108**, 17708–17713 (2011).
9. Wu, Y. *et al.* Spatially isotropic four-dimensional imaging with dual-view-plane illumination microscopy. *Nat. Biotechnol.* **31**, 1032–1038 (2013).
10. Kaufmann, A., Mickoleit, M., Weber, M. & Huisken, J. Multilayer mounting enables long-term imaging of zebrafish development in a light-sheet microscope. *Development* **139**, 3242–3247 (2012).
11. Vladimirov, N. *et al.* Light-sheet functional imaging in fictively behaving zebrafish. *Nat. Methods* **11**, 883–884 (2014).

12. Wolf, S. *et al.* Whole-brain functional imaging with two-photon light-sheet microscopy. *Nat. Methods* **12**, 379–380 (2015).

13. Pitrone, P.G. *et al.* OpenSPIM: an open-access light-sheet microscopy platform. *Nat. Methods* **10**, 598–599 (2013).

14. Gualda, E.J. *et al.* OpenSpinMicroscopy: an open-source integrated microscopy platform. *Nat. Methods* **10**, 599–600 (2013).

15. Huisken, J., Swoger, J., Del Bene, F., Wittbrodt, J. & Stelzer, E.H.K. Optical sectioning deep inside live embryos by selective-plane illumination microscopy. *Science* **305**, 1007–1009 (2004).

16. Huisken, J. & Stainier, D.Y.R. Even fluorescence excitation by multidirectional selective-plane illumination microscopy (mSPIM). *Opt. Lett.* **32**, 2608–2610 (2007).

17. Keller, P.J., Schmidt, A.D., Wittbrodt, J. & Stelzer, E.H.K. Reconstruction of zebrafish early embryonic development by scanned light-sheet microscopy. *Science* **322**, 1065–1069 (2008).

18. Chen, B.-C. *et al.* Lattice light-sheet microscopy: imaging molecules to embryos at high spatiotemporal resolution. *Science* **346**, 1257998 (2014).

19. Cella Zanacchi, F. *et al.* Live-cell 3D super-resolution imaging in thick biological samples. *Nat. Methods* **8**, 1047–1049 (2011).

20. Huang, B., Jones, S.A., Brandenburg, B. & Zhuang, X. Whole-cell 3D STORM reveals interactions between cellular structures with nanometer-scale resolution. *Nat. Methods* **5**, 1047–1052 (2008).

21. Gebhardt, J.C.M. *et al.* Single-molecule imaging of transcription factor binding to DNA in live mammalian cells. *Nat. Methods* **10**, 421–426 (2013).

22. Galland, R. *et al.* 3D high- and super-resolution imaging using single-objective SPIM. *Nat. Methods* **12**, 641–644 (2015).

23. Li, T. *et al.* Axial-plane optical microscopy. *Sci. Rep.* **4**, 7253 (2014).

24. Theer, P., Dragneva, D. & Knop, M. πSPIM: high-NA high-resolution isotropic light-sheet imaging in cell culture dishes. *Sci. Rep.* **6**, 32880 (2016).

25. Tokunaga, M., Imamoto, N. & Sakata-Sogawa, K. Highly inclined thin illumination enables clear single-molecule imaging in cells. *Nat. Methods* **5**, 159–161 (2008).

26. Gao, L. Optimization of the excitation light sheet in selective-plane illumination microscopy. *Biomed. Opt. Express* **6**, 881–890 (2015).

27. Planchon, T.A. *et al.* Rapid three-dimensional isotropic imaging of living cells using Bessel beam plane illumination. *Nat. Methods* **8**, 417–423 (2011).

28. Gao, L. *et al.* Non-invasive imaging beyond the diffraction limit of 3D dynamics in thickly fluorescent specimens. *Cell* **151**, 1370–1385 (2012).

29. Manton, J.D. & Rees, E.J. triSPIM: light-sheet microscopy with isotropic super-resolution. *Opt. Lett.* **41**, 4170–4173 (2016).

30. Zhao, T. *et al.* Multicolor 4D fluorescence microscopy using ultrathin Bessel light sheets. *Sci. Rep.* **6**, 26159 (2016).

31. Vettenburg, T. *et al.* Light-sheet microscopy using an Airy beam. *Nat. Methods* **11**, 541–544 (2014).

32. Zong, W. *et al.* Large-field high-resolution two-photon digital-scanned light-sheet microscopy. *Cell Res.* **25**, 254–257 (2015).

33. Dean, K.M. & Fiolka, R. Uniform and scalable light-sheets generated by extended focusing. *Opt. Express* **22**, 26141–26152 (2014).

34. Dean, K.M., Roudot, P., Welf, E.S., Danuser, G. & Fiolka, R. Deconvolution-free subcellular imaging with axially swept light-sheet microscopy. *Biophys. J.* **108**, 2807–2815 (2015).

35. Buytaert, J.A. & Dirckx, J.J. Design and quantitative resolution measurements of an optical virtual sectioning three-dimensional imaging technique for biomedical specimens, featuring two-micrometer slicing resolution. *J. Biomed. Opt.* **12**, 14039 (2011).

36. Gao, L. Extend the field of view of selective-plane illumination microscopy by tiling the excitation light sheet. *Opt. Express* **23**, 6102–6111 (2015).

37. Fu, Q., Martin, B.L., Matus, D.Q. & Gao, L. Imaging multicellular specimens with real-time optimized tiling light-sheet selective-plane illumination microscopy. *Nat. Commun.* **7**, 11088 (2016).

38. Friedrich, M., Gan, Q., Ermolayev, V. & Harms, G.S. STED-SPIM: stimulated emission depletion improves sheet-illumination microscopy resolution. *Biophys. J.* **100**, L43–L45 (2011).

39. Hoyer, P. *et al.* Breaking the diffraction limit of light-sheet fluorescence microscopy by RESOLFT. *Proc. Natl. Acad. Sci. USA* **113**, 3442–3446 (2016).

40. Palero, J., Santos, S.I.C.O., Artigas, D. & Loza-Alvarez, P. A simple scanless two-photon fluorescence microscope using selective plane illumination. *Opt. Express* **18**, 8491–8498 (2010).

41. Truong, T.V., Supatto, W., Koos, D.S., Choi, J.M. & Fraser, S.E. Deep and fast live imaging with two-photon scanned light-sheet microscopy. *Nat. Methods* **8**, 757–760 (2011).

42. Tomer, R., Khairy, K., Amat, F. & Keller, P.J. Quantitative high-speed imaging of entire developing embryos with simultaneous multiview light-sheet microscopy. *Nat. Methods* **9**, 755–763 (2012).

43. Lemon, W.C. *et al.* Whole-central nervous system functional imaging in larval *Drosophila*. *Nat. Commun.* **6**, 7924 (2015).

44. Supatto, W., Truong, T.V., Débarre, D. & Beaurepaire, E. Advances in multiphoton microscopy for imaging embryos. *Curr. Opin. Genet. Dev.* **21**, 538–548 (2011).

45. Ji, N., Magee, J.C. & Betzig, E. High-speed, low-photodamage nonlinear imaging using passive pulse splitters. *Nat. Methods* **5**, 197–202 (2008).

46. Mahou, P., Vermot, J., Beaurepaire, E. & Supatto, W. Multicolor two-photon light-sheet microscopy. *Nat. Methods* **11**, 600–601 (2014).

47. Fahrbach, F., Simon, P. & Rohrbach, A. Microscopy with self-reconstructing beams. *Nat. Photonics* **4**, 780–785 (2010).

48. Fahrbach, F.O., Gurchenkov, V., Alessandri, K., Nassoy, P. & Rohrbach, A. Self-reconstructing sectioned Bessel beams offer submicron optical sectioning for large fields of view in light-sheet microscopy. *Opt. Express* **21**, 11425–11440 (2013).

49. Fahrbach, F.O., Gurchenkov, V., Alessandri, K., Nassoy, P. & Rohrbach, A. Light-sheet microscopy in thick media using scanned Bessel beams and two-photon fluorescence excitation. *Opt. Express* **21**, 13824–13839 (2013).

50. Keller, P.J. *et al.* Fast, high-contrast imaging of animal development with scanned light-sheet-based structured-illumination microscopy. *Nat. Methods* **7**, 637–642 (2010).

51. Fahrbach, F.O. & Rohrbach, A. Propagation stability of self-reconstructing Bessel beams enables contrast-enhanced imaging in thick media. *Nat. Commun.* **3**, 632 (2012).

52. Silvestri, L., Bria, A., Sacconi, L., Iannello, G. & Pavone, F.S. Confocal light-sheet microscopy: micron-scale neuroanatomy of the entire mouse brain. *Opt. Express* **20**, 20582–20598 (2012).

53. Baumgart, E. & Kubitscheck, U. Scanned light-sheet microscopy with confocal slit detection. *Opt. Express* **20**, 21805–21814 (2012).

54. Yang, Z. *et al.* Dual-slit confocal light-sheet microscopy for *in vivo* whole-brain imaging of zebrafish. *Biomed. Opt. Express* **6**, 1797–1811 (2015).

55. de Medeiros, G. *et al.* Confocal multiview light-sheet microscopy. *Nat. Commun.* **6**, 8881 (2015).

56. Verveer, P.J. *et al.* High-resolution three-dimensional imaging of large specimens with light-sheet-based microscopy. *Nat. Methods* **4**, 311–313 (2007).

57. Preibisch, S., Saalfeld, S., Schindelin, J. & Tomancak, P. Software for bead-based registration of selective-plane illumination microscopy data. *Nat. Methods* **7**, 418–419 (2010).

58. Schmid, B. & Huisken, J. Real-time multiview deconvolution. *Bioinformatics* **31**, 3398–3400 (2015).

59. Preibisch, S. *et al.* Efficient Bayesian-based multiview deconvolution. *Nat. Methods* **11**, 645–648 (2014).

60. Swoger, J., Verveer, P., Greger, K., Huisken, J. & Stelzer, E.H.K. Multiview image fusion improves resolution in three-dimensional microscopy. *Opt. Express* **15**, 8029–8042 (2007).

61. Krzic, U., Gunther, S., Saunders, T.E., Streichan, S.J. & Hufnagel, L. Multiview light-sheet microscope for rapid *in toto* imaging. *Nat. Methods* **9**, 730–733 (2012).

62. Reynaud, E.G., Peychl, J., Huisken, J. & Tomancak, P. Guide to light-sheet microscopy for adventurous biologists. *Nat. Methods* **12**, 30–34 (2015).

63. Dodt, H.-U. *et al.* Ultramicroscopy: three-dimensional visualization of neuronal networks in the whole mouse brain. *Nat. Methods* **4**, 331–336 (2007).

64. Saghafi, S., Becker, K., Hahn, C. & Dodt, H.U. 3D-ultramicroscopy utilizing aspheric optics. *J. Biophotonics* **7**, 117–125 (2014).

65. Golub, I., Chebbi, B. & Golub, J. Toward the optical 'magic carpet': reducing the divergence of a light sheet below the diffraction limit. *Opt. Lett.* **40**, 5121–5124 (2015).

66. Wilding, D. *et al.* Pupil filters for extending the field of view in light-sheet microscopy. *Opt. Lett.* **41**, 1205–1208 (2016).

67. Tomer, R., Ye, L., Hsueh, B. & Deisseroth, K. Advanced CLARITY for rapid and high-resolution imaging of intact tissues. *Nat. Protoc.* **9**, 1682–1697 (2014).

68. Fahrbach, F.O., Voigt, F.F., Schmid, B., Helmchen, F. & Huisken, J. Rapid 3D light-sheet microscopy with a tunable lens. *Opt. Express* **21**, 21010–21026 (2013).

69. Ahrens, M.B., Orger, M.B., Robson, D.N., Li, J.M. & Keller, P.J. Whole-brain functional imaging at cellular resolution using light-sheet microscopy. *Nat. Methods* **10**, 413–420 (2013).

70. Olarte, O.E., Andilla, J., Artigas, D. & Loza-Alvarez, P. Decoupled illumination detection in light-sheet microscopy for fast volumetric imaging. *Optica* **2**, 702 (2015).

71. Quirin, S. *et al.* Calcium imaging of neural circuits with extended depth-of-field light-sheet microscopy. *Opt. Lett.* **41**, 855–858 (2016).

72. Tomer, R. *et al.* SPED light-sheet microscopy: fast mapping of biological system structure and function. *Cell* **163**, 1796–1806 (2015).

73. Dunsby, C. Optically sectioned imaging by oblique-plane microscopy. *Opt. Express* **16**, 20306–20316 (2008).

74. Bouchard, M.B. *et al.* Swept confocally aligned planar excitation (SCAPE) microscopy for high-speed volumetric imaging of behaving organisms. *Nat. Photonics* **9**, 113–119 (2015).

75. Jahr, W., Schmid, B., Schmied, C., Fahrbach, F.O. & Huisken, J. Hyperspectral light-sheet microscopy. *Nat. Commun.* **6**, 7990 (2015).

76. Cutrale, F. *et al.* Hyperspectral phasor analysis enables multiplexed 5D *in vivo* imaging. *Nat. Methods* **14**, 149–152 (2017).

77. Ji, N. Adaptive optical-fluorescence microscopy for biological imaging. *Nat. Methods* http://dx.doi.org/10.1038/nmeth.4218 (2017).

78. Masson, A. *et al.* High-resolution in-depth imaging of optically cleared thick samples using an adaptive SPIM. *Sci. Rep.* **5**, 16898 (2015).

79. Wilding, D., Pozzi, P., Soloviev, O., Vdovin, G. & Verhaegen, M. Adaptive illumination based on direct wavefront sensing in a light-sheet fluorescence microscope. *Opt. Express* **24**, 24896–24906 (2016).

80. Simmonds, R.D. & Booth, M.J. Modelling of multiconjugate adaptive optics for spatially variant aberrations in microscopy. *J. Opt.* **15**, 094010 (2013).

81. Royer, L.A. *et al.* Adaptive light-sheet microscopy for long-term, high-resolution imaging in living organisms. *Nat. Biotechnol.* **34**, 1267–1278 (2016).

82. Scherf, N. & Huisken, J. The smart and gentle microscope. *Nat. Biotechnol.* **33**, 815–818 (2015).

83. Hoebe, R.A. *et al.* Controlled light-exposure microscopy reduces photobleaching and phototoxicity in fluorescence live-cell imaging. *Nat. Biotechnol.* **25**, 249–253 (2007).

84. Conrad, C. *et al.* Micropilot: automation of fluorescence-microscopy-based imaging for systems biology. *Nat. Methods* **8**, 246–249 (2011).

85. Chmielewski, A.K. *et al.* Fast imaging of live organisms with sculpted light sheets. *Sci. Rep.* **5**, 9385 (2015).

86. Prevedel, R. *et al.* Simultaneous whole-animal 3D imaging of neuronal activity using light-field microscopy. *Nat. Methods* **11**, 727–730 (2014).

87. McGorty, R. *et al.* Open-top selective-plane illumination microscope for conventionally mounted specimens. *Opt. Express* **23**, 16142–16153 (2015).

88. Chung, K., Crane, M.M. & Lu, H. Automated on-chip rapid microscopy, phenotyping and sorting of *C. elegans*. *Nat. Methods* **5**, 637–643 (2008).

89. Pardo-Martin, C. *et al.* High-throughput hyperdimensional vertebrate phenotyping. *Nat. Commun.* **4**, 1467 (2013).

90. Pardo-Martin, C. *et al.* High-throughput *in vivo* vertebrate screening. *Nat. Methods* **7**, 634–636 (2010).

91. Gualda, E.J. *et al.* SPIM-fluid: open source light-sheet-based platform for high-throughput imaging. *Biomed. Opt. Express* **6**, 4447–4456 (2015).

92. Heemskerk, I. & Streichan, S.J. Tissue cartography: compressing bio-image data by dimensional reduction. *Nat. Methods* **12**, 1139–1142 (2015).

93. Guan, Z. *et al.* Compact plane illumination plugin device to enable light-sheet fluorescence imaging of multicellular organisms on an inverted wide-field microscope. *Biomed. Opt. Express* **7**, 194–208 (2015).

94. Paiè, P., Bragheri, F., Bassi, A. & Osellame, R. Selective-plane illumination microscopy on a chip. *Lab Chip* **16**, 1556–1560 (2016).

95. Engelbrecht, C.J., Voigt, F. & Helmchen, F. Miniaturized selective-plane illumination microscopy for high-contrast *in vivo* fluorescence imaging. *Opt. Lett.* **35**, 1413–1415 (2010).

96. Plöschner, M. *et al.* Multimode fiber: light-sheet microscopy at the tip of a needle. *Sci. Rep.* **5**, 18050 (2015).

97. Oshima, Y. *et al.* Light-sheet-excited spontaneous Raman imaging of a living fish by optical sectioning in a wide-field Raman microscope. *Opt. Express* **20**, 16195–16204 (2012).

98. Rocha-Mendoza, I. *et al.* Rapid spontaneous Raman light-sheet microscopy using cw lasers and tunable filters. *Biomed. Opt. Express* **6**, 3449–3461 (2015).

99. Yang, Z., Downie, H., Rozbicki, E., Dupuy, L.X. & MacDonald, M.P. Light sheet tomography (LST) for *in situ* imaging of plant roots. *Opt. Express* **21**, 16239–16247 (2013).

100. Mayer, J. *et al.* OPTiSPIM: integrating optical projection tomography in light-sheet microscopy extends specimen characterization to nonfluorescent contrasts. *Opt. Lett.* **39**, 1053–1056 (2014).

101. Bassi, A., Schmid, B. & Huisken, J. Optical tomography complements light-sheet microscopy for *in toto* imaging of zebrafish development. *Development* **142**, 1016–1020 (2015).

102. Doerr, J. *et al.* Whole-brain 3D mapping of human neural transplant innervation. *Nat. Commun.* **8**, 14162 (2017).

103. Engelbrecht, C.J. *et al.* Three-dimensional laser microsurgery in light-sheet-based microscopy (SPIM). *Opt. Express* **15**, 6420–6430 (2007).

104. Yang, Z., Piksarv, P., Ferrier, D.E.K., Gunn-Moore, F.J. & Dholakia, K. Macro-optical trapping for sample confinement in light-sheet microscopy. *Biomed. Opt. Express* **6**, 2778–2785 (2015).

105. Fahrbach, F.O. & Rohrbach, A. A line-scanned light-sheet microscope with phase-shaped self-reconstructing beams. *Opt. Express* **18**, 24229–24244 (2010).